

Steel-Free Hybrid FRP Stiffened Panel-Concrete Deck System

by L. Cheng and V.M. Karbhari

Synopsis: This paper presents a design, analysis, and characterization of a hybrid deck system incorporating a thin Fiber Reinforced Polymer (FRP) stiffened hat-panel configured stay-in-place formwork that serves as flexural reinforcement with steel-free concrete poured on top. Quasi-static tests were conducted to first investigate the flexural behavior of the system. To understand the deck performance under traffic loads that induce repetitive stress cycles during the service life, a two-span continuous deck specimen (1.22 m wide) was tested by subjecting it to a total of 2.36 million cycles of load that simulates an AASHTO design truck with inclusion of the impact factor at both low and high magnitudes. The concrete-panel interfacial response due to the presence of sand and interlocking ribs was characterized by performing a series of 610 mm wide deck section tests, the results of which were used to calibrate a finite-element (FE) based analytical model. The effect of the shear span-to-depth ratio, carbon fiber reinforcement ratio, and rib spacing were then evaluated by performing a parametric study using the calibrated nonlinear FE model. A simplified design approach is also proposed.

Keywords: analysis; bridge deck; characterization; fiber reinforced polymer (FRP); finite element (FE); steel-free

632 Cheng and Karbhari

Lijuan (Dawn) Cheng is a graduate research assistant in the Department of Structural Engineering at the University of California, San Diego. She is currently a PhD candidate and also a member of ASCE, SAMPE and ACI.

Vistasp M. Karbhari is a professor in the Department of Structural Engineering at the University of California, San Diego.

INTRODUCTION

As a result of the large percentage of concrete bridges in the United States that are structurally deficient due to corrosion of the embedded steel reinforcement and attendant concrete degradation in the bridge deck (Plecnik 1991), rapid replacement or rehabilitation methods are strongly desired. Developing new modular systems that consist of readily replaceable deck modules and that utilize high performance materials, such as advanced fiber reinforced polymer composites, is a potential solution to accomplish this. FRP composites are beneficial in bridge construction due to their high strength-to-weight ratio, low maintenance cost, and greatly increased durability with higher corrosion resistance compared to conventional steel reinforced concrete (RC) decks. However, in order to have any new system using innovative material stand up in the construction field, the evaluation of their application in prototype structures is essential so as to demonstrate their construction and performance capacity will achieve the designer's objectives.

Research on the application of FRP composites in bridge decks has advanced promisingly during the past twenty years. They have been considered as replacements for steel reinforcement in the concrete slabs in the form of tendons by Hassan et al. (2000), as 2D or 3D continuous grids and gratings by Yost and Schmeckpeper (2001), and as flat panels by Reising et al. (2001). Bridge decks consisting of pure polymer composites have also been studied by Karbhari et al. (2000). Due to the fact that the strength of a highway bridge deck is sensitive to repeated stressing, the fatigue behavior of bridge decks has also been extensively studied by Karbhari et al. (2000), GangaRao et al. (1999), Matsui et al. (2001), and Kwon et al. (2003). This paper is an attempt in the same direction, wherein the static and dynamic behavior of a recently developed hybrid modular deck system that is free of steel reinforcement and combines FRP composites and concrete material was evaluated. In this system, a steel-free concrete slab is cast on top of a carbon fiber reinforced FRP stiffened deck panel (as shown in Figure 1) that serves as both the flexural reinforcement and stay-in-place form for the concrete slab. To enhance the slab-deck interaction, the panel surface is sand treated and installed with discrete shear ribs. The objective of this study is to fully characterize the structural response of this prototype FRP-concrete deck system via a combination of analytical simulation and full-scale experimental investigation on the static flexural-shear response and the fatigue behavior under moving traffic loads. A finite element based analytical model was developed that demonstrated good agreement with the static test results; this was further utilized to perform a general parametric study of the system considering the

critical design variables such as the shear span-to-depth ratio and the amount of carbon fiber reinforcement. The major results of this research work are discussed herein.

STATIC RESPONSE

Materials and setup

The composite deck panel, as shown in Figure 1, consists of a bottom plate (2.254 m long and 6.3 mm thick) with end hooks for slab-girder connection and adhesively bonded rectangular stiffeners filled with foam. The bottom plate is composed of 8 layers of unidirectional carbon fabric with an areal weight of 305 g/m^2 and 4 layers of E-glass chopped strand mat with an areal weight of 458 g/m^2 , in a symmetric lay-up scheme of $[C/E/C_2/E/C]_s$. The rectangular stiffeners contain primarily unidirectional carbon fabric and foam core and are adhesively bonded onto the bottom plate. To enhance the shear interaction between the concrete slab and deck panel, the top surface of the panel is sand treated and additionally installed with shear ribs made of sand-epoxy paste. Five 610 mm wide testing specimens (SF1–SF5) were constructed from a steel-free concrete slab and such deck panel with different spacing for rectangular stiffeners and interfacial ribs (as summarized in Table 1). All the specimens were constructed with casting steel reinforced concrete blocks at both ends to simulate the condition of fixity to the supporting girders. The test setup is illustrated in Figure 2, where the specimen was simply supported by a roller at one end, a pin at the other, and quasi-statically loaded at mid-span from the top under a double-rod hydraulic actuator through an elastomeric loading pad up to different service and strength levels in relation to the AASHTO wheel load (98 kN), which is the AASHTO's HS-20 truck wheel load of 73 kN with the consideration of an impact factor of 33%. A load factor of 1.75 was used for STRENGTH I design level according to AASHTO (2004).

Observations and results

The displacement and strain response, crack pattern, and failure mode of each specimen were monitored during the test. The first three specimens (SF1–SF3) had a similar structural behavior with a stiffener spacing of 305 mm on center in each. Flexural cracks were found to first grow vertically near the bottom of slab at mid-span when the load reached 98 kN. As the load increased, additional cracking occurred at the locations of the interfacial ribs and further propagated diagonally toward the load point, as shown in Figure 3, due to the combined effect of flexural and shear stresses, i.e. principal tensile stresses. A sudden flexure-shear crack occurred in the slab at failure at a load carrying capacity similar among the three specimens, regardless of the spacing of the ribs. This is mainly due to the existence of the concrete end blocks at the ends, which provided a restraining effect from the ends such that the shear force could still be transferred from the slab to the deck even without the ribs at the interface. The ultimate capacity of SF4 with a stiffener spacing of 610 mm and SF6 without stiffeners were found to be about 17% and 43%, respectively, lower than that of the control panel SF1, indicating a significant effect of the spacing of the stiffeners on the global flexural capacity of the entire deck. Both specimens failed in a very similar flexure-shear mode as before. These cracks were found to propagate into the concrete end blocks in all the specimens except for SF1. The load vs. mid-span displacement response is shown in Figure 4 and Figure 5,

634 Cheng and Karbhari

where a largely linear-elastic behavior can be seen up to the ultimate load level that reached approximately twice the factored AASHTO wheel load demand for all the specimens (STRENGTH I, as represented by the top dashed line in the figure). The compressive strains in the concrete slab and tensile strains in the carbon fiber composite panel were all found to satisfy the code specified limit of 0.003 for concrete (ACI 1995) and the design specified allowable of 0.005 for carbon fiber reinforced composite at strength level (simplified recommendation for CFRP in the current design with the consideration of a reasonably large safety factor).

FATIGUE BEHAVIOR

Test configuration

The test specimen was constructed from two 1220 mm wide, 2254 mm long, and 6.3 mm thick FRP composite deck panels placed side-by-side, with a 196 mm thick steel-free concrete slab cast on top of the panels. The double span was selected for the specimen construction in order to include the continuity effect in the slab as would be experienced in the field application. A layer of carbon fiber reinforced mesh/grid was embedded in the concrete close to the top surface of the section at the middle one-third span region, serving as the tensile reinforcement at the negative bending moment region. The specimen was simply supported and loaded in a sinusoidal waveform by two 1828.8 mm apart patch loads of 84 kN via two double-rod hydraulic actuators to simulate one axle of the AASHTO truck wheel load while considering the dynamic load allowance factor. The setup configuration and the loading protocol are shown in Figure 6 and Figure 7, respectively. The specimen underwent 2.1 million cycles of fatigue service load and 250,000 cycles of doubled and 10,000 cycles of tripled fatigue load, after which the specimen was monotonically loaded up to failure. Deflections and strains were monitored using linear potentiometers and lead attached strain gages.

Results and discussion

During the fatigue stage, no tensile cracks were observed on the vertical sides of the specimen. Hairline cracking only formed on the top surface of the slab above the middle support at the end of the 2 million cycles of fatigue service load. The crack width satisfied the serviceability limit state per the code requirement. The maximum deflection of the structure under fatigue service load was found to be within the deflection-to-span ratio limit per the design code specification, satisfying the serviceability limit state with respect to the deflection limit. The structure had suffered no stiffness degradation during the first 2 million cycles of fatigue service load based on the small variation in the observed structural response. However, a substantial degradation of 37.6% was found during the subsequent 250,000 cycles of doubled fatigue service load and 44% during the further 10,000 cycles of tripled load (see Figure 8), indicating the higher the magnitude of the wheel load, the larger the amount of degradation in the system. The residual displacement in the system under all the fatigue load conditions was found to be insignificant and display a largely elastic and stable manner as seen in Figure 9, indicating no slippage at the slab-deck interface. The tensile strain and compressive strain experienced in the FRP composites and concrete material were found to be well below the design allowables. The existence of the carbon fiber composite mesh/grid that

was embedded in the middle support of the negative bending moment region was found to be beneficial in controlling the crack width and post cracking behavior of the concrete slab. Therefore, a minimum amount of fiber mesh is highly recommended and should be designed based on the concrete tensile stress demand in those regions.

PARAMETRIC STUDY

Objectives

The inclined flexural-shear type of failure as discussed in the previous static tests is mainly caused by the combined shear and flexure, which is affected by many principal variables including the shear span-to-depth ratio, the amount of carbon fiber reinforcement, the spacing of the shear ribs, the tensile strength of concrete, the size of deck, the axial forces applied on the section, etc. Extensive experimental tests on these effects are desired but oftentimes not economically allowed due to the high cost of composite panels and the time-consuming nature of the lab tests. In addition, the flexure-shear failure load is hard to predict using conventional reinforced concrete theories since the stress state in the cracked section varies as the crack propagates from flexure to shear, which causes a stress concentration near the head of the crack. For this reason, therefore, a semi-analytical/semi-empirical approach is developed in this study with the major objectives of: a) experimentally characterizing the sand-rib interfacial property through shear bond-slippage tests; b) developing a refined analytical model that is validated by experimental results; c) performing a parametric study using the refined analytical model to evaluate the effect of selected design parameters.

Shear bond experiment

Three deck sections (SB1, SB2 and SB3), that each had the same slab width as previous but a slightly shorter span length (2.024 m instead of 2.254 m), were constructed without casting the reinforced concrete blocks at the ends so as to allow for the slippage at the interface between the slab and deck panel. Additionally, in order to examine the spacing effect of the shear ribs, the three specimens were designed to have a different rib spacing of 152 mm, 305 mm, and infinity (i.e. no ribs at all), respectively (see Table 1). A similar setup configuration to those for the static flexure tests was adopted here. Quasi-static cycles were included in the loading protocol during the tests in an attempt at detecting the interface debonding using the so-called modal vibration device. Measurements on the mid-span displacement, strain levels in composites and concrete, and slippage along the span length of the specimens were taken during the tests. Similar flexural-shear type of cracking was observed in SB1 and SB2, but specimen SB3 failed in a more flexure like mode. Horizontal cracking or debonding was observed at the interface between the concrete slab and the deck panel and it occurred much earlier in SB3 than the other two specimens. The ultimate capacities of SB1 and SB2 were found to be close to each other while SB3 showed a much lower capacity of about 37% (Figure 10). This is mainly attributed to the existence of the shear ribs that proved to be sufficient to provide the shear transferring between the slab and the panel. The displacement and strain levels experienced in SB3 are hence smaller than the other two, as seen in Figure 11.

Analytical model

An analytical model was created using the general-purpose finite element analysis software ABAQUS (2003). Figure 12 illustrates the assembled components and the mesh scheme of a half-span deck model utilizing symmetry. The composite deck panel was modeled with 4-node doubly curved general-purpose shell elements with reduced integration points (S4R) and 8-node linear brick elements (C3D8) were used for the modeling of the concrete slab. Linear elastic orthotropic properties were assumed for the composites. The concrete damaged plasticity model in ABAQUS was used to model the nonlinear behavior of concrete. This model uses the concepts of isotropic damaged elasticity in combination with isotropic tensile and compressive plasticity to represent the inelastic behavior of concrete.

Two mechanical characteristics exist at the interface between the concrete slab and the composite deck panel, i.e., the sand-bond surface and the shear rib feature. The former introduced a friction effect at the interface and the latter results in an interlocking or dowel type of mechanism that provides a much larger contribution than friction. To model the friction, the basic classical Coulomb friction model was selected in ABAQUS combined with the definition of surface interaction, where the two contacting surfaces are assumed to carry shear stresses up to a certain magnitude across their interface before they start sliding relative to one another. This stress is defined as critical shear stress τ_{crit} , at which sliding of the surfaces starts as a fraction of the contact pressure p between the surfaces ($\tau_{crit} = \mu p$), where μ is known as the coefficient of friction and was experimentally measured as 0.562 for this specific type of sand-bond surface. Figure 13a gives a two-dimensional representation for this model. The shear ribs at the interface were modeled with spring elements, which act between the node of panel and the node of slab, with its line of action being the line joining the two nodes. The relative displacement along this line stands for the relative slippage between the two surfaces. The behavioral property of the springs was represented by a proposed bond strength-slippage relationship as illustrated in Figure 13b. The springs are assumed to behave linear elastically before reaching their ultimate capacity. After that, a sudden failure occurs in them with a sudden load drop and the spring stiffness (i.e., force per relative displacement) goes down to zero. The spring stiffness during the elastic range, k , is defined by the shear bond strength of the interface, which was assumed to be 50 MPa/mm based on the experimental data for CFRP-concrete interface from the reference by Yoshizawa et al. (2000). The ultimate shear strength τ_{ult} is governed by the nominal shear strength of a typical epoxy resin. The failure modes considered in the analysis include the followings: (a) tensile failure in the carbon FRP composite in the deck panel when the strain level reaches the maximum allowable design limit that is defined as 50% of the maximum level (i.e., $\varepsilon_{cf} = 0.5 \times 0.01 = 5000 \mu\epsilon$); (b) compressive failure due to crushing in concrete at the top-of-slab when the compressive strain in concrete reaches the code specified ultimate level, i.e., $\varepsilon_{cu} = -3000 \mu\epsilon$ (ACI 1995); (c) inclined flexural-shear failure when the diagonal shear crack forms, i.e., the maximum principal stress along the path of the crack, σ_{max} , exceeds the tensile strength of concrete, f_{ct} ; (d) anchorage failure in ribs when the shear stress in springs exceeds the ultimate level as aforementioned.

Figure 14 and Figure 15 compare the analytically obtained mid-span displacement and maximum strain response with the experimental data in SB1, which shows a fairly good correlation between them but with a larger analytical load capacity than the test. This is mainly due to the fact that multiple sequences were introduced into the loading protocol through the entire test up to failure, which resulted in large stiffness degradation in the system because of the accumulated damages, and in turn, hindered the specimen from reaching its ultimate capacity, as it should have if monotonic load was applied up to failure. Due to the use of the concrete damaged plasticity model that is not based on the smeared crack approach, the notion of cracks developed in the slab was not visualizable. However, by introducing the concept of effective crack direction, a graphical visualization of the cracking patterns can be obtained, the results of which on SB1 is compared in Figure 16. The direction of the vector normal to the crack plane is parallel to the direction of the maximum principal plastic strain and the length of the colored vector is proportional to the amount of cracking. Concrete crushing was analytically obtained at ultimate strain, at which stage the potential formation of inclined crack was seen from the principal stress contour as shown in Figure 17. The maximum shear stress in the interfacial ribs was found to be much smaller than the ultimate strength. The developed analytical model was further verified via comparisons with test results from SB2. The load-displacement response and crack pattern are displayed in Figure 18 and Figure 19.

Design parameters

The inclined cracking behavior of the FRP-concrete deck is affected by many variables of which only a subset is studied herein, including the tensile strength of concrete (f_{ct}), the shear span-to-depth ratio (a/d), the amount of carbon fiber reinforcement (ρ_c), and the spacing of the ribs (s). The other geometrical and material parameters, such as the depth of the slab and the modulus of composites, had the same values as the current design and remained constants during the parametric study. It is known that the tensile strength of concrete (f_{ct}) can be directly related to the compressive strength (f_c') and also the typical range of f_c' for bridge deck application is from 16.5 MPa to 68.9 MPa, according to AASHTO. Two boundary cases and another typical design with f_c' equal to 43.9 MPa were selected here. The shear span-to-depth ratio (a/d) in concrete members without vertical stirrups has been found to likely determine the type of failure experienced in the member (MacGregor 1997). For this reason, a range from 2.5 to 6.5 was selected for a/d , in which cases the inclined flexural-shear type of failure typically occurs. The number of carbon fiber reinforcement layers at the bottom of the deck panel was allowed to vary from 4 layers to 12 layers, resulting in a plate total thickness within [4.37–7.42 mm]. The symmetry design in the laminate was maintained for all the cases. Two types of rib spacing were considered, namely, 152 mm and 305 mm. The deck system without shear ribs at the panel surface is not recommended based on the poor structural response observed in the test.

Figure 20 demonstrates the effect of different concrete strengths on the load-displacement response of the system. It can be seen that the load capacity can be increased 68.3% by changing the concrete strength from 16.5 MPa to 43.9 MPa and about 25.9% from 43.9 MPa to 68.9 MPa, indicating a larger gain in capacity as concrete strength increases at

638 Cheng and Karbhari

lower strength levels. The influence of the carbon fiber amount is illustrated in Figure 21 and Figure 22 for different rib spacings. The load capacity increases very linearly after the carbon fiber amount is increased up to 6 layers. Figure 23 and Figure 24 show the effect of shear span-to-depth ratio on the load capacity, which decreases quite uniformly as the deck gets slender. Slight differences in the load capacity can be seen between the deck with a rib spacing of 152 mm and the one with 305 mm, but is less substantial compared to the effect of the other variables.

DESIGN APPROACH

Composite deck panel

During the construction stage before the concrete sets, the composite deck panel itself should be designed to carry the concrete deck load, the composite deck dead load, and the construction live load. The maximum stress and strain levels in the deck for bending and shear can be computed by elastic theory from its sectional properties and moment and deflection coefficients determined from static analysis based on classical beam theory.

Shear-bond strength

As previously mentioned, the inclined shear crack loads are very difficult to predict due to the change in stress state within the cracked section. Therefore, a semi-empirical equation combining analytical simulations and statistical regression analysis is developed in this study to calculate the inclined shear capacity for the deck system. The ACI Building Code (1995) provides a shear equation in a form similar to the modified equation adopted herein as equation (1), which is based on the hypothesis that failure is initiated by the diagonal tension cracking,

$$\frac{V_u s}{b d} = \frac{m \rho d}{L'} + k \sqrt{f'_c} \quad (1)$$

In equation (1), V_u is the shear load, b is the deck width, and d is the distance from the extreme compressive fiber to the centroid of the deck. The reinforcement percentage, ρ , is given by A_s/bd . L' is the shear span length and f'_c is the compressive strength of concrete. The parameters, m and k , are the constants that are typically determined from an empirical fit to testing data. The term s accounts for the spacing of the shear transferring ribs. In this study, the specimen cases (60 in total) developed for the parametric study, where the analytical model was finely validated from the experimental tests, were used in deriving the shear design equation. A plot is made of the parameter, $V_u s/(bd\sqrt{f'_c})$, as ordinates X and $\rho d/(L'\sqrt{f'_c})$ as abscissas Y (see Figure 25). Two separate linear regressions are then performed with respect to the two rib spacing cases to determine the slope, m , and the zero intercept, k . In order to account for the insufficient specimen cases and variations that occur in the numerical results, a reduced regression line obtained by reducing the slope and intercept, respectively, of the original regression by 15% is proposed. The design equations as such obtained are given as follows,

$$\left\{ \begin{array}{l} \frac{V_u s}{b d} = \frac{19.983 \rho_c d'}{L'} + 0.0139 \sqrt{f'_c} \quad (\text{for rib spacing } s=152 \text{ mm}) \quad (2a) \\ \frac{V_u s}{b d} = \frac{44.509 \rho_c d'}{L'} + 0.0206 \sqrt{f'_c} \quad (\text{for rib spacing } s=305 \text{ mm}) \quad (2b) \end{array} \right.$$

The confidence level of both of the regression analyses was about 95% and the R^2 statistic or the coefficient of determination for these equations is about 0.63 and 0.88, respectively. By combining dimensional analysis techniques with statistical regression analysis, alternative design formula by Zsutty (1968) uses an expression involving an exponent of one-third of the parameters $(f'_c \rho_c d'/L')$ in the following form

$$\frac{V_u s}{bd'} = m \left(\frac{f'_c \rho_c d'}{L'} \right)^{1/3} + k \quad (3)$$

Following the similar procedure as before, a plot was made of the parameter $(f'_c \rho_c d'/L')^{1/3}$ as abscissa X and $V_u s/(bd')$ as ordinate Y, and the design equations thus obtained are described by Eq. (5-6) with better R-square values of 0.92 and 0.91 for cases with a rib spacing of 152 mm and 305 mm, respectively. These equations should be recommended for the use in the design.

$$\left\{ \begin{array}{l} \frac{V_u s}{bd'} = 0.750 \left(\frac{f'_c \rho_c d'}{L'} \right)^{1/3} - 0.366 \quad (\text{for rib spacing } s=152 \text{ mm}) \\ \frac{V_u s}{bd'} = 1.511 \left(\frac{f'_c \rho_c d'}{L'} \right)^{1/3} - 0.770 \quad (\text{for rib spacing } s=305 \text{ mm}) \end{array} \right. \quad (4a)$$

$$\left\{ \begin{array}{l} \frac{V_u s}{bd'} = 0.750 \left(\frac{f'_c \rho_c d'}{L'} \right)^{1/3} - 0.366 \quad (\text{for rib spacing } s=152 \text{ mm}) \\ \frac{V_u s}{bd'} = 1.511 \left(\frac{f'_c \rho_c d'}{L'} \right)^{1/3} - 0.770 \quad (\text{for rib spacing } s=305 \text{ mm}) \end{array} \right. \quad (4b)$$

Flexural strength

The flexural capacity of the deck system can be obtained from the compatibility of strains and the equilibrium of internal forces along the section (see Figure 26), following the similar principle as that for the reinforced concrete structures. The controlling strain herein is either the maximum compressive strain of 0.003 in concrete or the allowable tensile strain of 0.005 in carbon fiber composites. The nominal moment strength, M_u , is obtained as a simple summation of internal moments of all the tensile and compressive forces on the cross section that is considered. Other design considerations such as deflection limitation should also be included.

SUMMARY

An extensive testing program has been conducted on a new deck system, which was based on the concept of using hybrid FRP-concrete materials with modular construction. The static flexure-shear response and the fatigue behavior of the system have been fully characterized, and the results were found to meet the code specified limits and requirements. A finite element based analytical approach was developed and the validity as well as the accuracy of this approach has been well demonstrated through the comparisons of the results with the experimental data. A parametric study primarily concerned with the design variables of concrete strength, shear span-to-depth ratio, carbon fiber amount, and shear rib spacing was performed.

Since only a very thin layer of CFRP composite plate (6 mm) is used in the 203 mm thick concrete slab, the material cost in the proposed system is comparable to the conventional RC system and other currently available steel-free concrete deck systems. Also considering the cost savings from installing and demolding the formwork for the concrete slab and the associated cost-consuming labor, as the construction of

640 Cheng and Karbhari

conventional RC deck would have, the overall market cost of this system is very competitive. Additional cost savings can be gained in the long-term maintenance cost during the service-life of the structure due to the significantly improved durability in the proposed system.

Based on the findings from the current study, the following notes shall be recommended for the design of this deck system: (a) The rectangular stiffeners on the deck panel should not be designed to carry the construction load only, but also should take into account the flexural strength of the entire FRP-concrete deck system; (b) Based on the fatigue behavior of the deck system, the fatigue limit state was found to be not a governing state in the design as long as a minimum amount of composite fiber mesh was provided at regions where concrete tensile stress exists; (c) Eq. (4) can be utilized to design the shear-bond strength for the FRP-concrete deck system.

The range of the parametric study herein was selected for the current research interests. Extension of this range to other existing variables, such as the concrete strength, and inclusion of further parameters, such as the depth of the slab, can be included in future work. Other potential effort can be focused on the long-term behavior of the deck system due to creep and shrinkage, and the temperature and moisture environment.

REFERENCES

- AASHTO LRFD Bridge Design Specifications* (2004), 3rd Edition, American Association of State Highway and Transportation Officials, Washington, D.C.
- ABAQUS/Standard User's Manual (2003), Version 6.4, ABAQUS Inc.
- ACI 318-95 (1995), Building Code Requirements for Structural Concrete (ACI 318-95) and Commentary (ACI 318R-95), American Concrete Institute, Farmington Hills, MI.
- GangaRao, H.V.S., Thippeswamy, H.K., Shekar, V., and Craigo, C. (1999), "Development of Glass Fiber Reinforced Polymer Composite Bridge Deck," *SAMPE Journal*, 35(4): 12-24.
- Hassan, T., Abdelrahman, A., Tadros, G., and Rizkalla, S. (2000), "Fibre reinforced polymer reinforcing bars for bridge decks," *Can. J. Civ. Eng.*, 27:839-849.
- Karbhari, V.M., Seible, F., Burgueno, R., Davol, A., Wernli, M. and Zhao, L. (2000), "Structural Characterization of Fiber-Reinforced Composite Short-and Medium-Span Bridge Systems," *Applied Composite Materials*, 7 (2/3), pp. 151-182.
- Kwon, S.C., Dutta, P.K., Kim, Y.H., and Lopez-Anido, R. (2003), "Comparison of the fatigue behaviors of FRP bridge decks and reinforced concrete conventional decks under extreme environment conditions," *KSME International Journal*, 17(1): 1-10.

MacGregor, J.G. (1997), *Reinforced Concrete: Mechanics and Design*, 3rd edition, Prentice-Hall Inc., New Jersey.

Matsui, S., Ishizaki, S. and Kubo, K. (2001), "An Experimental Study on Durability of FRP-RC Composite Deck Slabs of Highway Bridges," *Proceedings of the 3rd International Conference on Concrete Under Severe Conditions: Environment & Loading*, Vancouver, Canada, pp. 933-940.

Plecnik, J.M., and Azar, W.A. (1991), "Structural components, highway bridge deck applications," *International Encyclopedia of Composites*, 6: 430-445.

Reising, R.M.W., Shahrooz, B.M., Hunt, V.J., Lenett, M.S., Christopher S., Neumann, A.R., Helmicki, A.J., Miller, R.A., Kondury, S., and Morton, S. (2001), "Performance of five-span steel bridge with fiber-reinforced polymer composite deck panels," *Transportation Research Record 1770*, Paper No. 01-0337, pp.113-123.

Yoshizawa, H., Wu, Z.S., Yuan, H., and Kanakubo, T. (2000), "Study on FRP-Concrete Interface Bond Performance," *Journal of Materials, Concrete Structures and Pavements, JSCE*, 49:662, pp. 105-119.

Yost, J.R. and Schmeckpeper, E.R. (2001), "Strength and serviceability of FRP grid reinforced bridge deck," *Journal of Bridge Engineering*, 6(6):605-612.

Zsutty, T.C. (1968), "Beam Shear Strength Prediction by Analysis of Existing Data," *Proceedings, Journal of the American Concrete Institute*, November, 65(11): 943-951.

Table 1 – Summary of static tests

Specimen Number	Stiffener Spacing on panel (mm)	Rib Spacing on panel (mm)	P_{ult} (kN)	δ at Failure (mm)	Failure Mode	Crack in End Block
SF1 [†]	305 (2 stiffeners)	152	311.6	16.8	Combined flexural and diagonal shear	None
SF2	305 (2 stiffeners)	305	316.4	17.9		Some
SF3	305 (2 stiffeners)	No ribs	302.6	17.2		Some
SF4	610 (1 stiffener)	152	258.2	13.6		None
SF5	No stiffener	152	179.2	15.1		Some
SB1 [†]	305 (2 stiffeners)	152	321.4	14.5	Flexure	No end block constructed
SB2	305 (2 stiffeners)	305	327.8	14.3		
SB3	305 (2 stiffeners)	No ribs	202.1	9.28		

* Control panel as originally designed. † SF – Flexural specimen; SB – Shear bond specimen

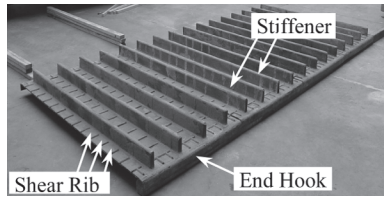


Figure 1 – Geometry of FRP composite deck panel

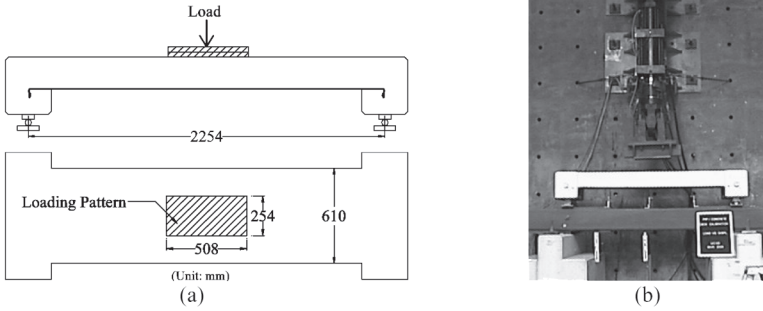


Figure 2 – (a) Geometry; (b) Configuration of static test setup

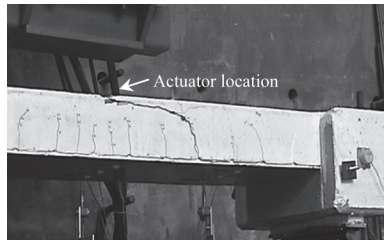


Figure 3 – Typical crack pattern for static test

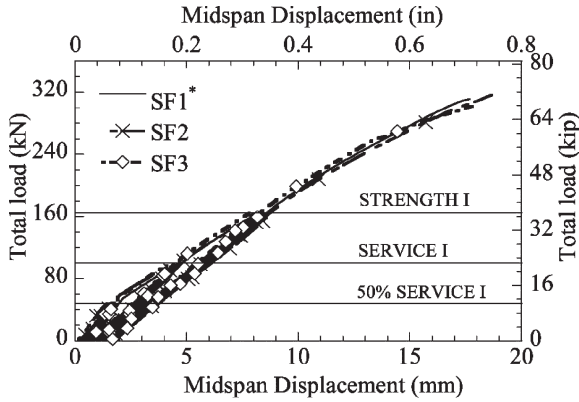


Figure 4 – Load vs. displacement response for SF1, SF2 and SF3

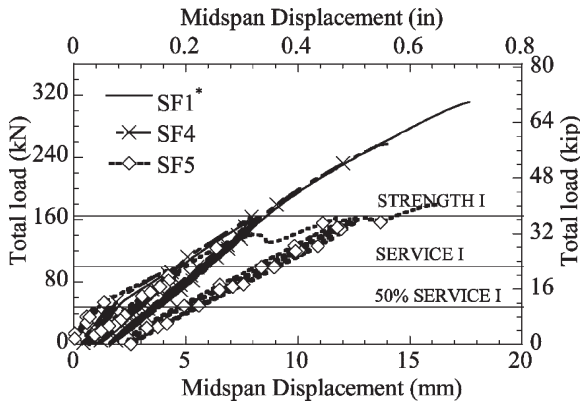


Figure 5 – Load vs. displacement response for SF1, SF4 and SF5

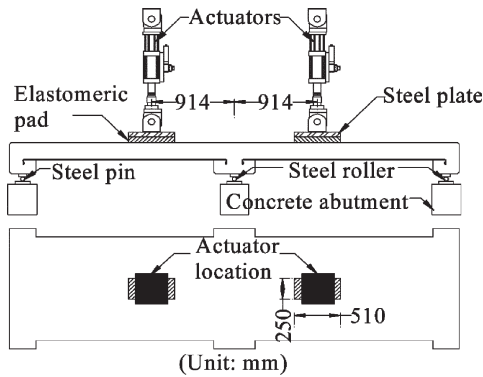


Figure 6 – Fatigue test setup

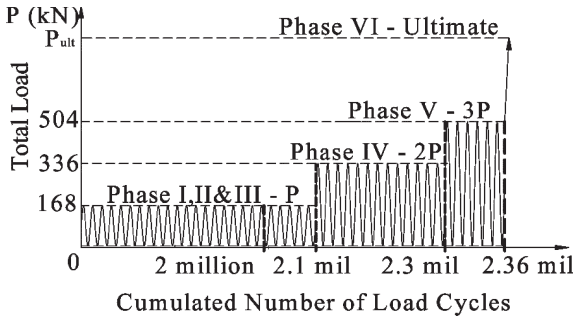


Figure 7 – Loading protocol for fatigue test

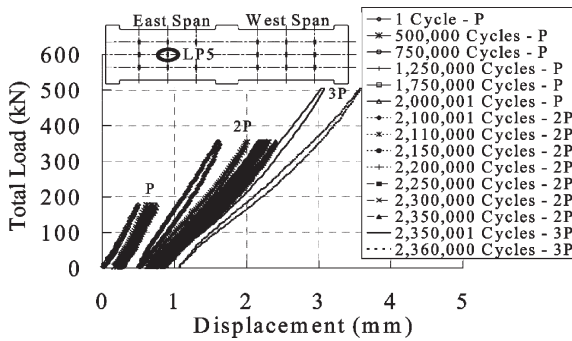


Figure 8 – Load-displacement response before ultimate for fatigue test

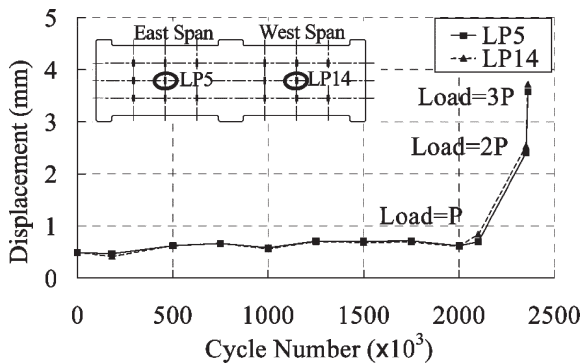


Figure 9 – Mid-span displacement history during fatigue test

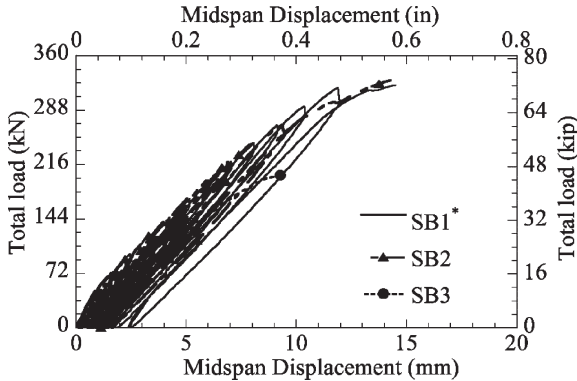


Figure 10 – Load-displacement response of shear-bond test

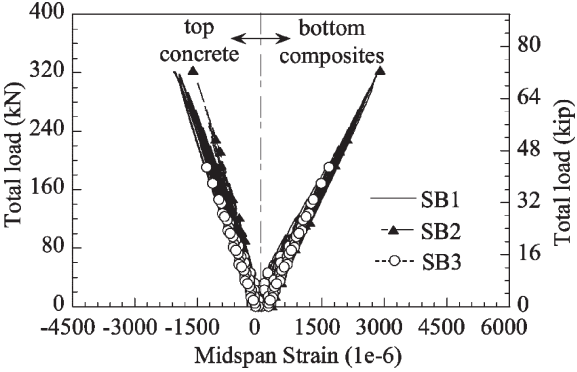


Figure 11 – Load-strain response of shear-bond test

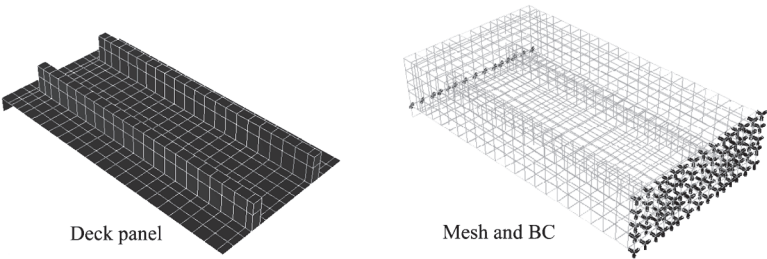


Figure 12 – Finite element modeling

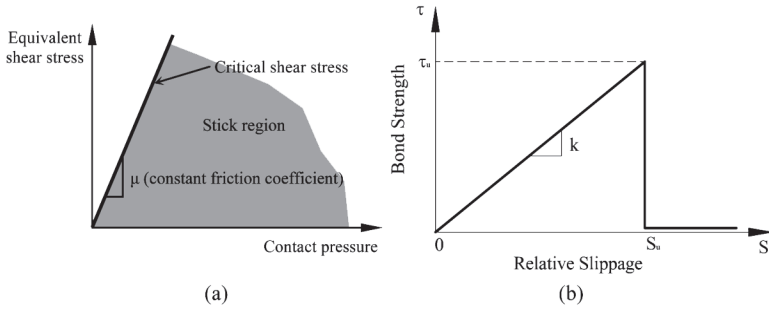


Figure 13 – (a) Friction model; (b) Proposed bond strength-slippage model

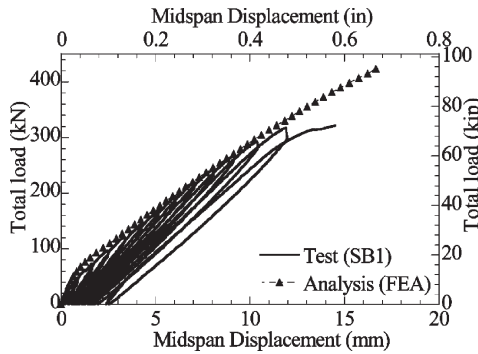


Figure 14 – Verification of FEA model for SB1 from the load-displacement response

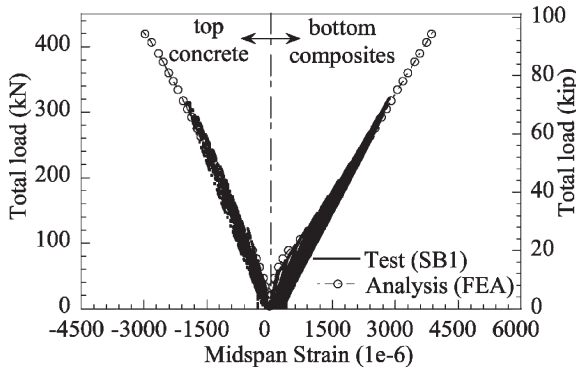


Figure 15 – Verification of FEA model for SB1 from load-strain response

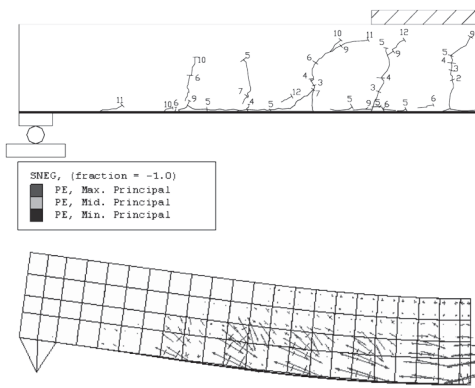


Figure 16 – Comparison of crack pattern in SB1

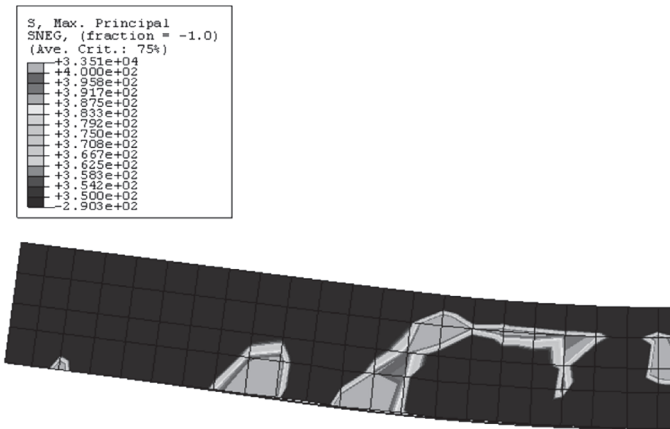


Figure 17 – Comparison of principal stress contour in SB1

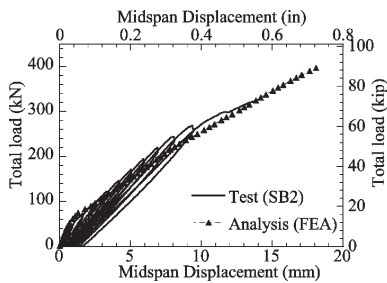


Figure 18 – Verification of FEA model for SB2 from the load-displacement response

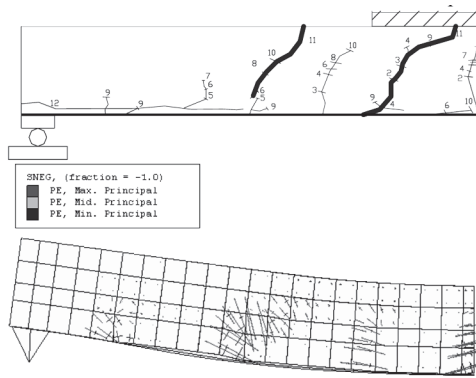


Figure 19 – Comparison of crack pattern in SB2

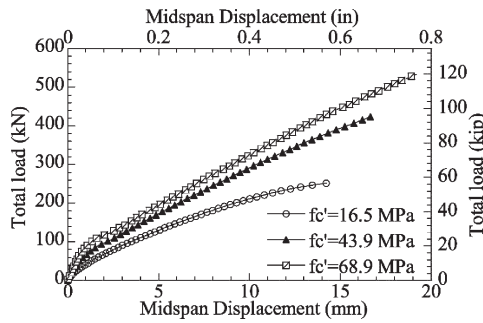


Figure 20 – Effect of concrete strength with rib spacing of 152 mm

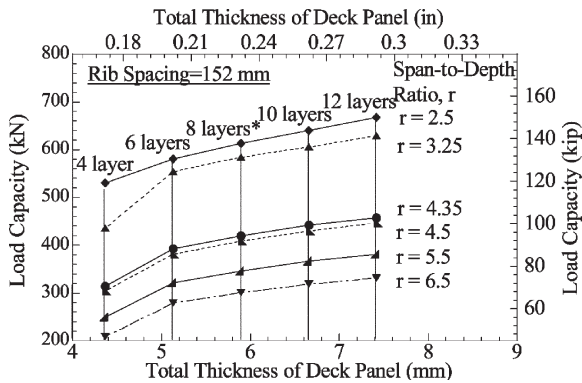


Figure 21 – Effect of carbon fiber amount for cases with rib spacing of 152 mm

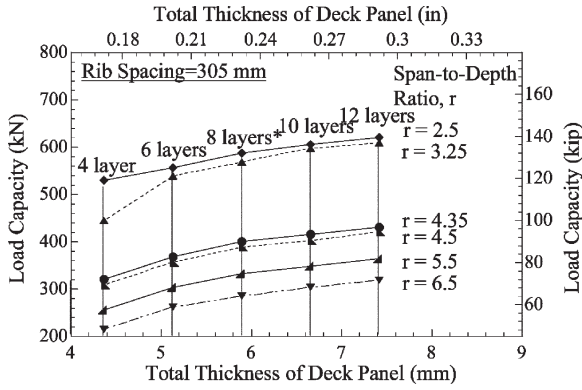


Figure 22 – Effect of carbon fiber amount for cases with rib spacing of 305 mm

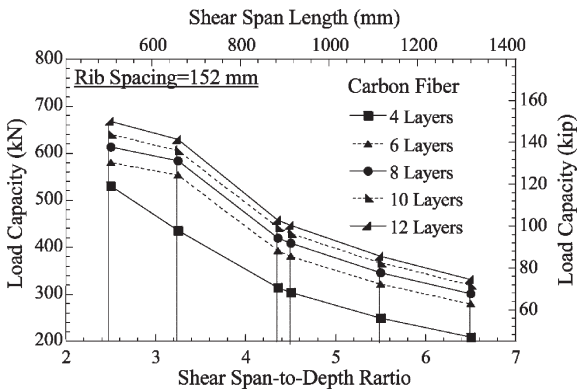


Figure 23 – Effect of span-to-depth ratio for cases with rib spacing of 152 mm

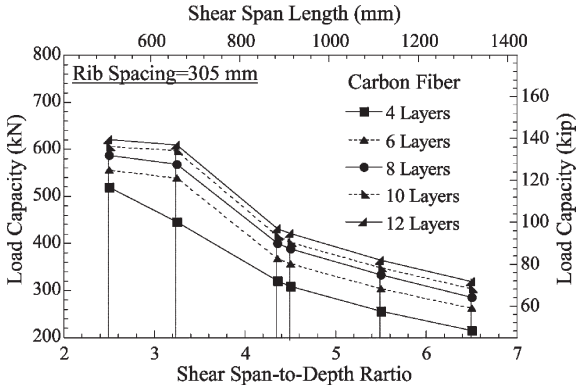


Figure 24 – Effect of span-to-depth ratio for cases with rib spacing of 305 mm

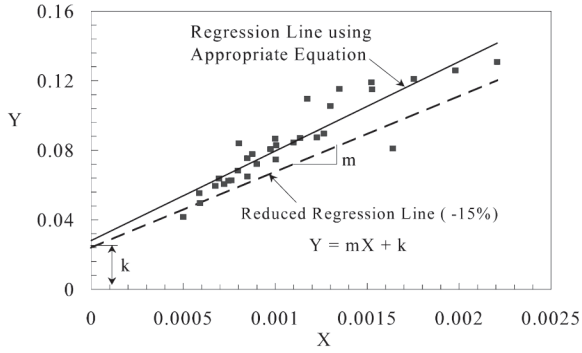


Figure 25 – Plot for regression analysis

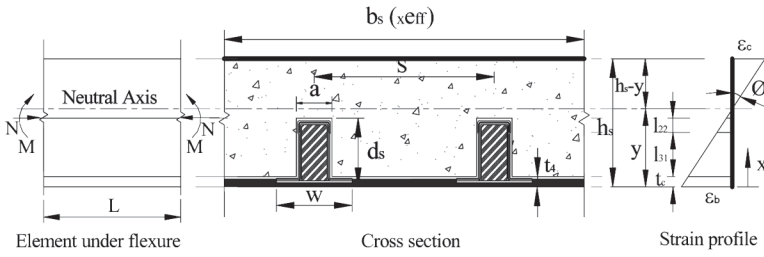


Figure 26 – Typical cross section of FRP-concrete deck system